



Li Reaction Mechanism of MnP Nanoparticles

Soojin Sim and Jaephil Cho^{*,z}

Interdisciplinary School of Green Energy and Converging Research Center for Innovative Battery Technologies,
Ulsan National Institute of Science and Technology (UNIST), Ulsan 689-798, Korea

MnP nanoparticles (MnPs) with a particle size of <30 nm were prepared by the reaction of dimanganese decacarbonyl and trioctyl phosphine (TOP) at 380°C under Ar atmosphere. Lithium reaction mechanism of the MnPs was investigated by using electrochemical cycling, ex situ X-ray diffraction (XRD) and Transmission Electron Microscopy (TEM). When lithium ion was first inserted into the MnP, it started to form LiMnP, LiP and LiP₇ phases. During lithium dealloying (charging to 2 V), LiMnP phase was turned into the LiP and LiP₅ phases.

© 2012 The Electrochemical Society. [DOI: 10.1149/2.081205jes] All rights reserved.

Manuscript submitted June 10, 2011; revised manuscript received February 15, 2012. Published March 12, 2012.

P-based compounds, especially metal phosphides (MP_x; M = Fe, Co, Cu, Zn, Sn, V, Ni, Mn, and Ti) have been studied as anode material candidates because of their high gravimetric and volumetric capacities. In addition, these materials showed the dynamic phase changes depending on the potential window.¹⁻⁸ MPs are categorized into two groups depending on their Li insertion mechanism. First are the compounds showing topotactic lithium reaction that maintains their pristine phase.^{3,9,10} Nazar et al. reported that lithium intercalation in MnP₄ occurred by an electrochemical redox process according to a reversible reaction MnP₄ ↔ Li₇MnP₄. The covalent P-P bonds in the MnP₄ are cleaved on Li insertion to produce crystalline Li₇MnP₄. Atom migration with bond rearrangement during lithium desorption lead to electrochemical recrystallization reforming MnP₄ between 0.57 and 1.7V.⁹ SnP_{0.94} also demonstrated simple intercalation mechanism without changing the Sn oxidation state and can accept 4.5 mole of Li into the material. (SnP_{0.94} + 4.5Li ↔ Li_{4.5}SnP_{0.94}).¹⁰ Similarly MoP₂ prepared by ballmilling of stoichiometric amount of Mo and P exhibits similar behaviors to SnP_{0.94} during lithium reaction and exhibited capacity of 822 mAh/g (Li_{5.2}MoP₂).³

The second group is compounds showing metal alloying/metallization reaction represented by the following decomposition reaction: MP_n ↔ M⁰ + Li_xP. Some examples are GaP,¹¹ FeP₂,¹² CoP₃,¹³ Cu₃P,¹⁴ VP₄,¹⁵ and ZnP₂.¹⁶ For instance, Li reaction in CoP₃ was proposed as follows: CoP₃ → Li₃P + Co → 3LiP + Co. Accordingly, the initial uptake of Li forms highly dispersed cobalt clusters embedded in a matrix of Li₃P; extraction of Li from this ion-conductive matrix on charging yields nanoparticles of LiP without oxidation of Co. LiP is an insulator, and once Li₃P changed into LiP in the above reaction, it had a detrimental effect on the reversibility of the phosphorus electrode.¹³ However, ZnP₂ have different lithium reaction mechanism which does not form Li₃P. ZnP₂ showed simple topotactic reaction until x = 2.6 in Li_xZnP₂, after which it decomposed to Zn, ZnP₂, LiZnP and LiP₅ phases between 2 and 0V. As a progress of charge, the LiP₅ and Zn are reformed to ZnP₂ and P, and finally they are turned to ZnP, P, LiP, and LiZnP.¹⁶

To the best of our knowledge, there have been no reports of lithium reaction mechanism of MnPs. Here we report the synthesis and lithium reaction mechanism of MnPs prepared by the reaction of dimanganese decacarbonyl and TOP at 380°C under Ar atmosphere.

Experimental

Orthorhombic MnPs were synthesized by a reflux method at 380°C in schlenk line. 1.5 g of Mn₂(CO)₁₀ (98%, Ardrich) is dissolved in 100 mL of TOP (90%, Ardrich) and heated with stirring for 2–4 h at 380°C. When the solution color was changed from yellow to black, it was cooled to a room temperature and that was rinsed with ethanol and chloroform with centrifuging 2 times at 5000 rpm in order to remove

the excess P sources of TOP. Finally, the black powder was vacuum dried at 90°C for one day. All the sample preparation was carried out in the glove box under the Ar atmosphere.

For the electrochemical tests, Coin-type half-cell tests were conducted, using MnP powder, Super P carbon black and poly(vinylidene fluoride) (PVdF) binder in a weight ratio of 70:20:10. The slurry was thoroughly mixed with N-methyl 2-pyrrolidinone (NMP). 1.05 M LiPF₆ in ethylene carbonate/dimethyl carbonate (EC/DMC) (1:1 vol%) was used as the electrolyte. The cell was assembled in an Ar-filled glove box. The cell was cycled at discharge and charge rates of 0.1 C (= 72 mA/g) and 0.05 C, respectively, between 0 and 2 V. The XRD measurements were performed using a Rigaku D/Max 200 with Cu Kα radiation at 10 kW. The sample was observed using a scanning electron microscope (SEM, JSM 6400, JEOL) and a transition electron microscope (TEM, JEOL 2010F). For the TEM measurement, lithiated and delithiated MnP samples were detached from the Cu electrode and was introduced into the glass vials containing ethanol or acetone. After ultrasonic treatment, a droplet of solvent was placed in carbon-coated copper grid. All these sample preparation was done in the glove box.

Results and Discussion

Figure 1 shows the powder X-ray diffraction pattern of MnPs, which can be indexed to an orthorhombic structure with a *Pmna* space group. Figure 2a exhibits the SEM images of the as-prepared MnPs, and it consists of aggregated nanoparticles with <100 nm. Figure 2b shows the TEM image of pristine MnPs and their primary particle sizes range between 5 nm and 30 nm. MnPs are surrounded by amorphous phase, and expanded images (Figs. 2c and 2d) of Fig. 2b exhibit the lattice fringes of (011) and (211) planes corresponding to *d*-spacing values of 2.74 Å and 1.94 Å of MnP, respectively. Energy dispersive X-ray spectra (EDXS) at spots 1 and 2 (Fig. 2e) confirm that amorphous region also consists of MnP phase (Fig. 2f).

Voltage profiles of the MnP electrode between 0 and 2 V at a rate of 0.1 C for discharge and 0.05 C for charge in coin-type lithium half cells at 21°C are illustrated in Figure 3a. The first discharge and charge capacities of the MnP were 1242 mAh/g and 361 mAh/g, respectively, showing irreversible capacity ratio of 70%. However, columbic efficiency of MnPs after 2nd cycle was almost 80% and displays relatively good capacity retention out to 10 cycles. Based upon its capacity estimate, the insertion amount of lithium ions is estimated to 4 mole per MnP (Li₄MnP) during the first lithiation to 0 V. Figures 3b and 3c shows the differential capacity plots (DCPs) of MnPs during the first and second cycles, respectively. DCPs show a sharp and a broad peak at 0.57 and 0.34 V, and two broad peaks at 0.7 and 1.1 V during the first discharge and charge cycles, respectively. In order to figure out such phase transitions, ex situ XRD experiments at selected potentials during the first cycle as indicated in Fig. 3a were carried out and results are given in Figure 4. Similar to XRD patterns of the bulk and nano-sized metal phosphides,^{1,2,5,6} our data

* Electrochemical Society Active Member.

^z E-mail: jphcho@unist.ac.kr

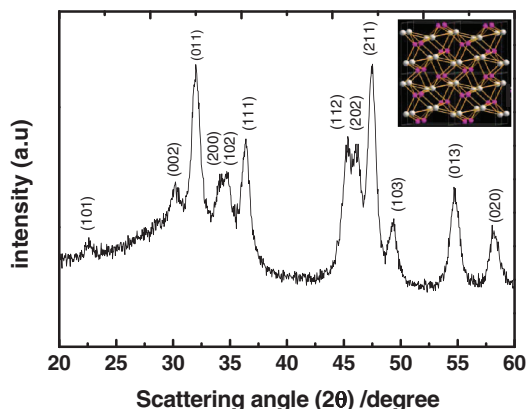


Figure 1. XRD patterns of the MnP nanoparticles. (#JCPDS = 78-0267) and an inset is orthorhombic MnP structure (pink = phosphorus, white = manganese).

also exhibit rather poor resolution with approaching higher degree of lithium intercalation/deintercalation. This phenomena is related to the formation of amorphous phases and particle pulverization.^{1,2,5,6} In spite of this, each peak can be clearly identified.

At point 2 (0.8 V), MnP phase start to decompose with concomitant formation of LiMnP phase and at point 3 (0.34 V), and LiMnP and LiP₇ phases get dominant. Digitalized Fourier-transformed image (DFTI) of MnP electrode after discharging at 0.34 V (point 3) also confirms the formation of LiMnP phase. Selected area diffraction pattern (Fig. 5b) of Fig. 5a shows ($\bar{1}10$) and ($\bar{1}02$) planes along the [221] zone axis, corresponding to tetragonal LiMnP phase. When it is further discharged to 0 V (point 4), peaks intensity of LiMnP decreases and LiP

and LiP₇ phases get dominant. Especially, LiP phase formation from the LiMnP phase should be accompanied by Mn phase according to a following reaction: $\text{LiMnP} \rightarrow \text{LiP} + \text{Mn}$. Although no clear evidence of Mn nanoparticles are observed from the analyzes, decomposed LiMnP phase may lend the formation of Mn phase. Other MPs, such as Cu₃P, CuP₂, NiP₂, VP₂, and CoP₃ were also proposed the formation of metal phase in spite of no direct evidence was supplied.^{13,17-21} During the first charge, complete disappearance of residual LiMnP phase at 0 V and increasing peaks intensities of LiP₅ and LiP₇ phases are noticeable (point 6). This means that LiMnP and LiP₇ phases are decomposed to LiP₅ and LiP phases. However, at point 7 (2 V), peaks intensities of LiP and LiP₅ phases get decreased, while any new peaks are detected. This result suggests the possible particle pulverization of LiP and LiP₅ phases.

Figure 6 shows high resolution TEM images and corresponding DFTI of the electrode after first discharge to 0 V. DFTI of point 1 confirms the presence of the LiP₇ which has (211) and (413) planes along the $[\bar{2}22]$ zone axis, and that of point 2 is matched with (220) and (004) phases along the $[8\bar{8}0]$ zone axis, and also correspond to LiP₇. Figures 7a and 7b exhibit TEM images after first charge to 2 V, and compared with TEM image of the pristine sample, particles are pulverized and some of them were grown into larger ones. DFTI at point 1 shows the presence of ($\bar{1}20$) and ($\bar{1}\bar{1}2$) phase along the [423] zone axis, and those planes correspond to LiP₅ phase. DFTIs of points 2 and 3 show ($\bar{1}\bar{1}\bar{1}$) and ($\bar{1}\bar{1}\bar{2}$) planes along the [110] zone axis, and (110) and (111) along the [112] zone axis, and these planes agree with those of LiP phase. These results agree with XRD patterns, and it can be proposed that both DCP peaks at 0.57 and 0.34 V during the first discharge are related to phase transitions from MnP to LiMnP and from LiMnP to LiP₇, respectively. The peaks at 0.7 and 1.1 V are believed to be related to phase transitions between LiP₅ and LiP₇. During the second cycle, DCP shows an absence of the sharp peak at

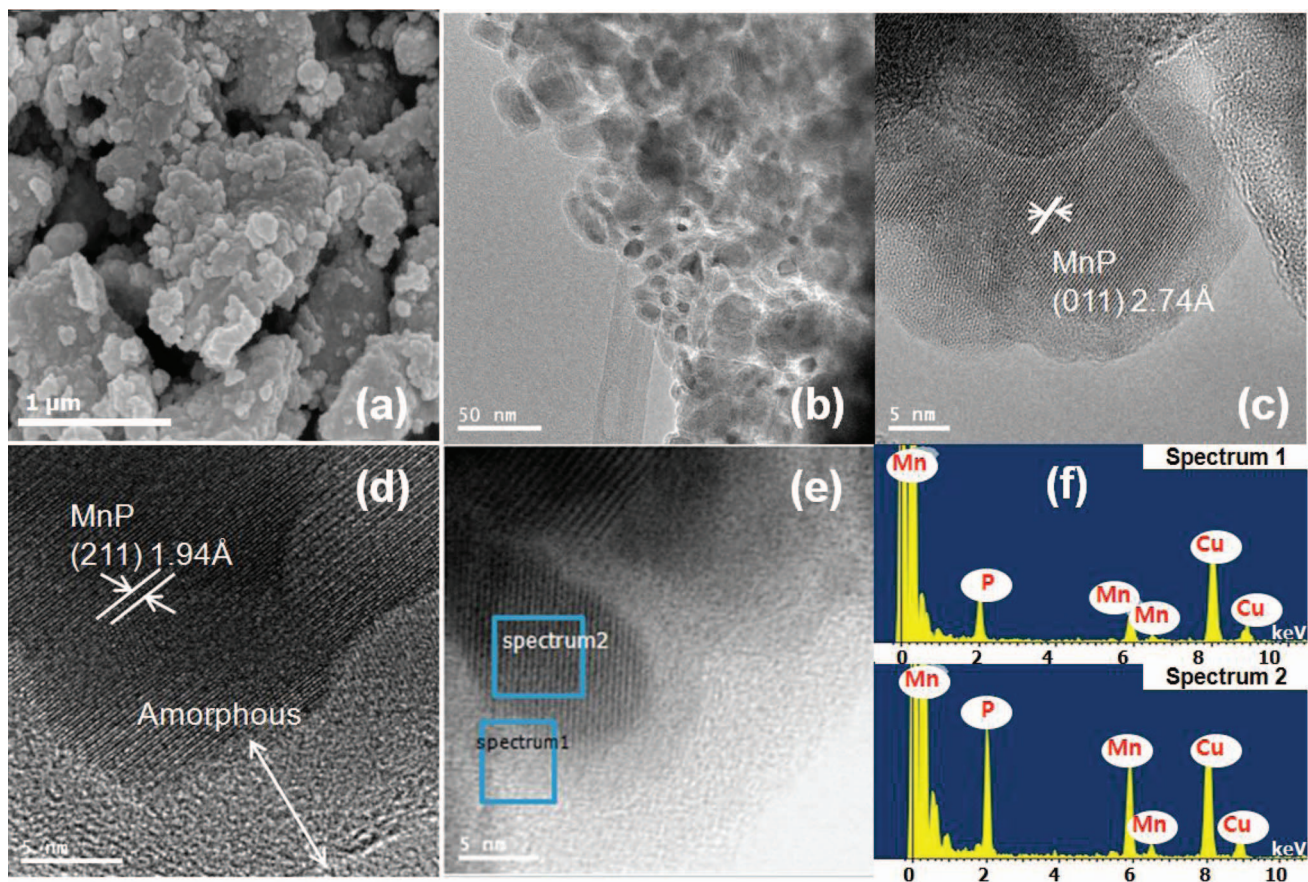


Figure 2. (a) SEM and (b, c, d, and e) TEM images and EDXS of pristine MnPs.

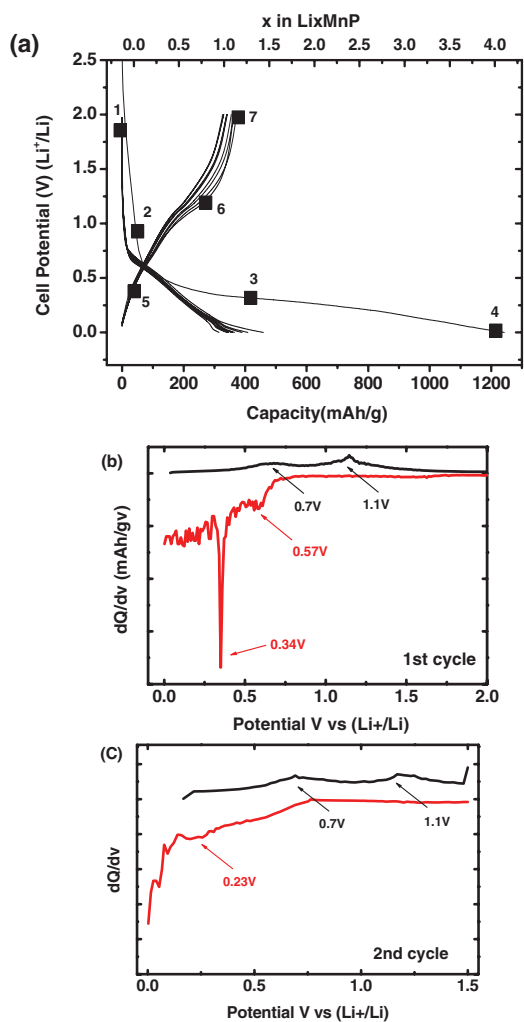


Figure 3. (a) Voltage curves of the MnP electrode between 2 and 0 V in a coin-type lithium half cell at rates of 0.1 and 0.05 C during the discharge and charge, respectively (numbers on the first charge and discharge curves indicates the voltages XRD patterns were taken) and (b) and (c) Differential capacity plots as a function of potential after (a) first and (b) second cycles.

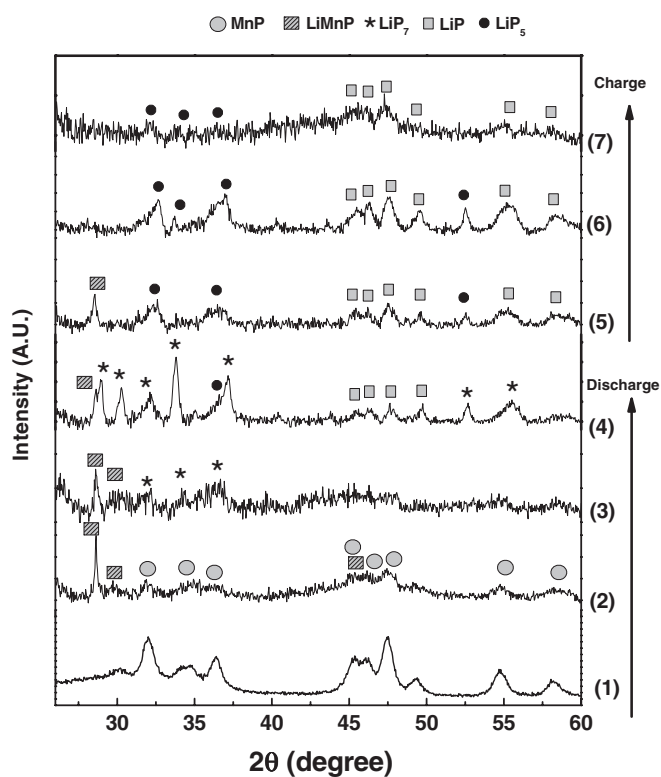


Figure 4. Ex situ XRD patterns of the MnP electrodes obtained from Fig. 3a.

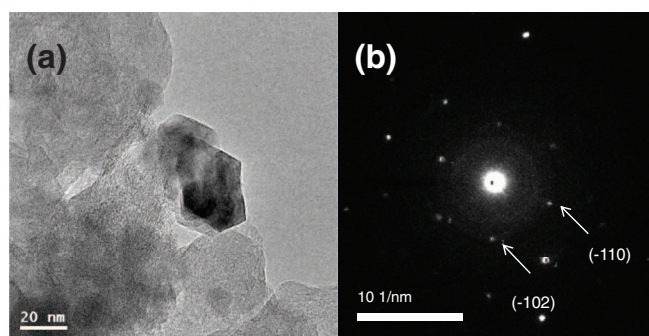


Figure 5. (a) High resolution image of MnP after discharging to 0.34 V and (b) selected area diffraction (SAD) pattern of (a).

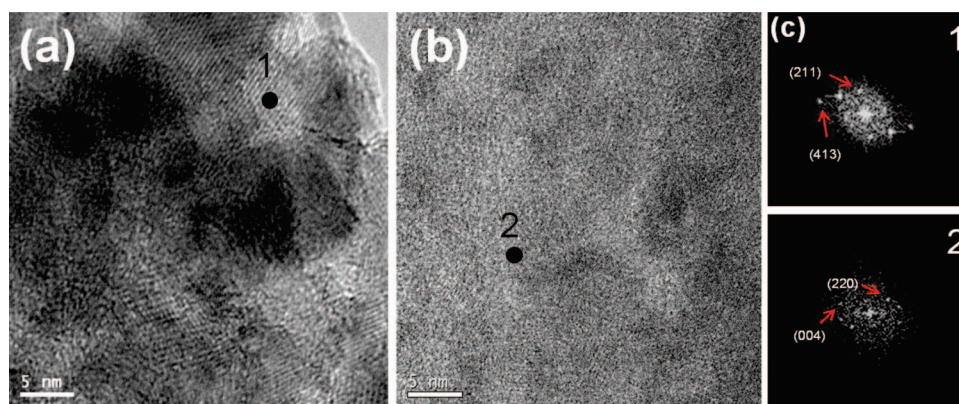


Figure 6. (c and d) TEM images of MnPs after discharge to 0 V, and (1 and 2) SAD patterns of (c and d) respectively.

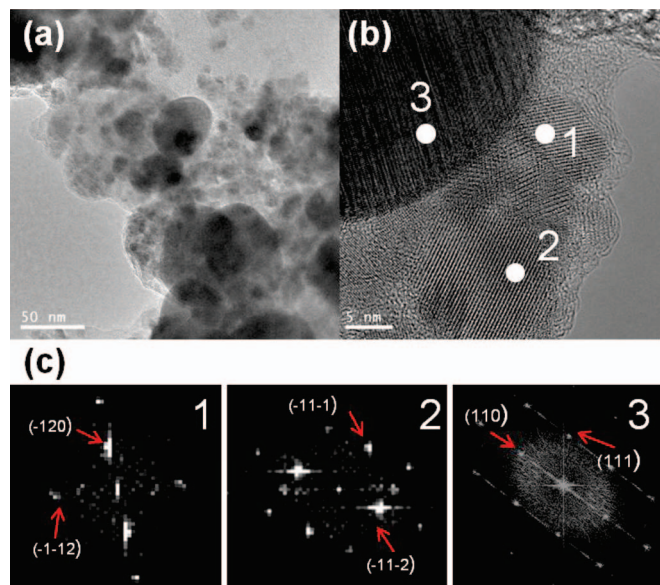


Figure 7. (a and b) TEM images of MnPs after charge to 2 V, and (1, 2, and 3) SAD patterns of the areas 1, 2 and 3 in (b).

0.34 V but other peaks intensities are quite similar to that of the first cycle. This means that phase transition between LiP and LiP₇ phases are relatively reversible. However, it should be noted that irreversible phase transitions of LiMnP phase to LiP_x phases, along with the formation of inactive LiMnP led to very low coulombic efficiency during the first cycle.

Figure 8a and 8b show the XRD pattern of the MnP electrodes after 2nd and 10 cycles respectively. After 10 cycles, both LiP_x phases are observed but their peak intensities decreased. This means that such phases are decomposed into P and Li or are pulverized to nanoparticles, leading to continuous capacity fading of MnP.

It has been reported that the most prevalent reasons for capacity fade in the metal alloys are 1) electrical disconnection of the electrode from the current collector caused by the compositional volume changes occurring during cycling, and as the particles fragment, they become electrically isolated, which reduces the cell capacity and 2) onset of the side reactions due to a slight instability of the phosphorus based reaction products with the present electrolytes, leading to some decomposition.²² Presently, the second reason is much more likely to

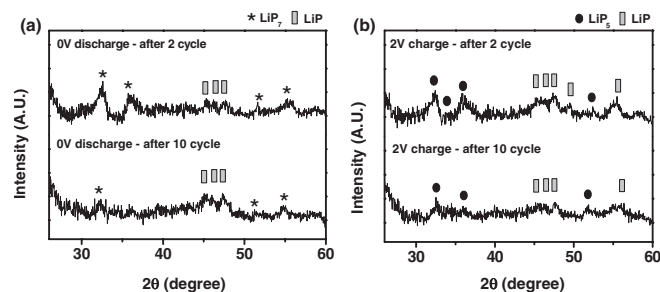


Figure 8. Ex situ XRD patterns of (a) the discharged and (b) the charged MnP electrodes to 0 V and 2 V after second and 10th cycles, respectively.

account for capacity loss in the metal phosphides because microstructure control did not affect the capacity enhancement.²³ Accordingly, electrolyte decomposition reactions catalyzed by LiP_x decomposition may enhance the cracking and crumbling of the electrode during cycling, resulting in a continuous generation of new active surfaces that were previously passivated by the stable surface films.

Conclusions

MnP nanoparticles with particle sizes of <30 nm were prepared by the simple thermal decomposition method. When lithium ion was first inserted into the MnP, it started to form LiMnP. However, LiMnP phase was decomposed to LiP and LiP₇ phases with decreasing the cell potential to 0 V. During lithium dealloying (charging to 2 V), LiMnP phase was turned into the LiP and LiP₅ phases. Low coulombic efficiency of the MnP nanoparticles during the first cycle was related to irreversible phase transitions of LiMnP phase to LiP_x phases. Decomposition and pulverization of the LiP_x phase led to continuous capacity fading of MnP.

Acknowledgments

This research was supported by the MKE (The Ministry of Knowledge Economy), Korea, under the ITRC (Information Technology Research Center) support program supervised by the NIPA (National IT Industry Promotion Agency) (NIPA-2012-C1090-1200-0002).

References

1. C.-M. Park, J.-H. Kim, H. Kim, and H.-J. Sohn, *Chem. Soc. Rev.*, **39**, 3115 (2010).
2. Y.-U. Kim, C. K. Lee, H.-J. Sohn, and T. Kang, *J. Electrochem. Soc.*, **151**, A933 (2004).
3. M. G. Kim, S. Lee, and J. Cho, *J. Electrochem. Soc.*, **156**, A89 (2009).
4. S. Boyanov, D. Zitoun, M. Ménétrier, J. C. Jumas, M. Womes, and L. Monconduit, *J. Phys. Chem. C*, **113**, 21441 (2009).
5. S. Boyanov, K. Annou, C. Villeveuille, M. Pelosi, D. Zitoun, and L. Monconduit, *Ionics*, **14**, 183 (2008).
6. S. Boyanov, J. Bernardi, E. Bekaert, M. Ménétrier, M. L. Doublet, and L. Monconduit, *Chem. Mater.*, **21**, 298 (2008).
7. M. G. Kim and J. Cho, *Adv. Funct. Mater.*, **19**, 1497 (2009).
8. F. Gillot, M. P. Bichat, F. Favier, M. Morcrette, M. L. Doublet, and L. Monconduit, *Electrochim. Acta*, **49**, 2325 (2004).
9. D. C. S. Souza, V. Pralong, A. J. Jacobson, and L. F. Nazar, *Science*, **296**, 2012 (2002).
10. Y. Kim, H. Hwang, C. Yoon, M. Kim, and J. Cho, *Adv. Mater.*, **19**, 92 (2007).
11. H. Hwang, M. G. Kim, and J. Cho, *J. Phys. Chem. C*, **111**, 1186 (2007).
12. D. C. C. Silva, O. Crosnier, G. Ouvrard, J. Greedan, A. Safa-Sefat, and L. F. Nazar, *Electrochem. Solid-State Lett.*, **6**, A162 (2003).
13. V. Pralong, D. C. S. Souza, K. T. Leung, and L. F. Nazar, *Electrochem. Comm.*, **4**, 516 (2002).
14. M. P. Bichat, T. Politova, J. L. Pascal, F. Favier, and L. Monconduit, *J. Electrochem. Soc.*, **151**, A2074 (2004).
15. Y.-U. Kim, B. W. Cho, and H.-J. Sohn, *J. Electrochem. Soc.*, **152**, A1475 (2005).
16. H. Hwang, M. G. Kim, Y. Kim, S. W. Martin, and J. Cho, *J. Mater. Chem.*, **17**, 3161 (2007).
17. B. Mauvernay, M. Bichat, F. Favier, L. Monconduit, M. Morcrette, and M. Doublet, *Ionics*, **11**, 36 (2005).
18. F. Gillot, S. Boyanov, L. Dupont, M. L. Doublet, M. Morcrette, L. Monconduit, and J. M. Tarascon, *Chem. Mater.*, **17**, 6327 (2005).
19. K. Wang, J. Yang, J. Xie, B. Wang, and Z. Wen, *Electrochem. Comm.*, **5**, 480 (2003).
20. B. Mauvernay, M. L. Doublet, and L. Monconduit, *J. Phys. Chem. Solids*, **67**, 1252 (2006).
21. F. Gillot, M. Ménétrier, E. Bekaert, L. Dupont, M. Morcrette, L. Monconduit, and J. M. Tarascon, *J. Power Sources*, **172**, 877 (2007).
22. R. Alcántara, J. L. Tirado, J. C. Jumas, L. Monconduit, and J. Olivier-Fourcade, *J. Power Sources*, **109**, 308 (2002).
23. O. Crosnier and L. F. Nazar, *Electrochem. Solid-State Lett.*, **7**, A187 (2004).